JOURNAL OF CATALYSIS 147, 500–514 (1994)

High Surface Area Platinum–Titania Aerogels: Preparation, Structural Properties, and Hydrogenation Activity

M. Schneider, D. G. Duff, T. Mallát, M. Wildberger, and A. Baiker[1]

Department of Chemical Engineering and Industrial Chemistry, Swiss Federal Institute of Technology, ETH-Zentrum, CH-8092 Zürich, Switzerland

Received September 29, 1993; revised December 9, 1993

High surface area platinum–titania aerogels with marked meso- to macroporosity have been synthesized via the sol–gel–aerogel route. An acid-catalyzed titania gel was prepared from tetrabutoxytitanium(IV) with methanol as solvent. The platinum precursor solutions added after the redispersion of the titania gel were either $PtCl_4$, $(NH_4)_2PtCl_6$ or $Pt(acac)_2$ dissolved in protic solvents. Platinum metal particles formed upon high-termperature supercritical drying. The platinum–titania aerogels have a BET surface area of 150 to 190 $m^2\ g^{-1}$ after thermal pretreatments up to 673 K and the titania matrix consists of well-developed anatase crystallites of about 8–9 nm mean size. Depending on the platinum precursor used, the volume-weighted-mean particle size, determined by TEM, varies in the range 3.6 to 68 nm, consistent with XRD results for the platinum component. All aerogel samples showed a pronounced stability of both the titania matrix and the platinum particles towards air or hydrogen at temperatures up to 673 K. Thermal analysis, combined with mass spectroscopy, revealed that the untreated catalysts contain a considerable amount of entrapped organic impurities after the high-temperature supercritical drying. For the characterization of the activity and the accessibility of platinum particles the liquid phase hydrogenations of *trans*-stilbene and benzophenone were used as test reactions. Compared to a commercial alumina-supported platinum catalyst, the untreated 2–5 wt% platinum–titania catalysts derived from $(NH_4)_2PtCl_6$- and especially $PtCl_4$- precursor solutions exhibit a markedly higher catalytic activity. In general, air pretreatments at 573 K or above had either no or promoting influence on activity. In contrast, pretreatments in hydrogen produced either no or detrimental activity change.

INTRODUCTION

Aerogel materials as catalysts go back to their discovery by Kistler in the 1930s (1, 2). A significant development came in the 1960s when Teichner and co-workers started to prepare aerogels by hydrolyzing metal alkoxides in alcoholic solutions (3–5), thereby drastically reducing the amount of water used and thus making the preparation of aerogels more feasible.

The potential of aerogels for catalysis resides in their unique morphological and chemical properties (6–8). These originate from their wet-chemical preparation by the solution–sol–gel (SSG) method (9) and the subsequent removal of solvent via supercritical drying (SCD). Due to the "structure-preserving" ability of SCD (10), the aerogels are usually solids of high porosity and specific surface area. They possess an ultrafine cell/pore size (<100 nm) and an ultrastructure of interconnected colloidal or polymeric primary particles of about 10 nm in size. The reductive alcoholic atmosphere during the high-temperature SCD further enables the simultaneous reduction of various ionic metal precursors to corresponding metallic particles (6, 11, 12). Moreover, co-gels of group VIII metals, highly dispersed in various metal oxide matrices, are readily prepared by sol–gel technology ensuring a uniform distribution of a metal throughout the solid, helping to prevent sintering and coking as well as improving the mechanical stability (6, 12–18). López *et al.* explain such enhanced performance mainly in terms of the more intimately developed metal–support interaction in comparison with conventionally impregnated catalysts. In essence, their preparation of metal–metal oxide xerogels involved adding the metal salt precursor solution (Pt, Pd, Ru, Rh) to the other reactants under reflux or vice versa. Besides the advantages mentioned, one should also note the fact that such molecularly mixed preparation routes allow for the incorporation of at least part of the precious metal component within the matrix (19–21), this being no longer accessible for catalytic processes.

To our knowledge, the preparation of Pt–titania aerogels has not so far been reported. In the last few years a marked commercial and academic interest has arisen with respect to titania as a possible support for metal (especially group VIII) catalysts in catalytic fine chemical synthesis (22–26). This is mainly due to the so-called strong metal support interactions (SMSI), reported for titania in particular (27, 28), which are supposed to be the reason for increased selectivity and/or activity in hydrogenation of various carbonyl groups (22–24, 26). At present the

[1] To whom correspondence should be addressed.

0021-9517/94 $6.00

most widely used catalyst-support materials in fine chemical synthesis are still carbon, alumina, and silica. Nevertheless, apart from the above-mentioned intrinsic advantages of aerogels themselves, such highly structured Pt–titania materials could offer interesting possibilities for various catalytic applications.

Recently we demonstrated that meso- to macroporous titania aerogels with high surface area can be synthesized by applying high-temperature SCD (29). This stimulated us to investigate the potential of this material as an alternative catalyst support in fine chemical synthesis, although in our preliminary investigations conventional impregnation with Pt salts afforded hardly any improvements. Thus, we developed a method for the direct synthesis of Pt–titania aerogels. Instead of mixing titanium and Pt components from the beginning of the SSG process, we tried to return to the "primary" structure of the titania matrix via redispersion of titania gels back to their colloidal state, hence giving us the advantage of homogeneously dispersing the metal precursor solution in the SSG sample. Another at least equally important aspect arises from the use of preformed colloidally dispersed titania, helping to prevent the incorporation of a significant part of the precious Pt particles (19–21).

The objective of this work was to prepare mesoporous Pt–titania aerogels with high specific surface areas suited for fine chemical catalysis. Starting with a fixed, well-established preparation scheme for the titania matrix (29), various Pt precursor solutions were added after the gelation stage. For the characterization of the availability and activity of Pt particles the liquid-phase hydrogenations of *trans*-stilbene [1] and benzophenone [2] were chosen:

$$\mathrm{Ph{-}CH{=}CH{-}Ph} \xrightarrow{+H_2} \mathrm{Ph{-}CH_2{-}CH_2{-}Ph} \qquad [1]$$

$$\mathrm{Ph{-}CO{-}Ph} \xrightarrow{+H_2} \mathrm{Ph{-}CHOH{-}Ph} \xrightarrow[-H_2O]{+H_2} \mathrm{Ph{-}CH_2{-}Ph.} \qquad [2]$$

Trans-stilbene and benzophenone are both bulky molecules favouring wide pores and they offer two different functional groups: C=C double bond and carbonyl group, respectively. Despite the ambient temperature liquid-phase hydrogenation, which is especially suitable for bulky molecules, we also investigated various pretreatment procedures with respect to future gas-phase reactions.

EXPERIMENTAL

Sol–Gel–Aerogel Synthesis

Throughout the text the following scheme of abbreviations is used (Pt2PC is here presented as an example): The numeral following "Pt" displays the Pt content in weight percent and the subsequent two capital letters represent the Pt precursor used ($PtCl_4$ → PC; $Pt(acac)_2$ → PA; $(NH_4)_2PtCl_6$ → NP). The thus-derived acronyms stand for the original (untreated) aerogel material.

Analytical grade reagents were used throughout this work. The preparation of the titania gels basically followed that of aerogel C in (29). In brief, the SSG-process was carried out in an antiadhesive, closed teflon beaker, under nitrogen atmosphere and at ambient temperature (297 ± 2 K). Two solutions were prepared. The first solution consisted of 32.0 g tetrabutoxytitanium(IV) (TBOT) dissolved in 120 ml methanol and the second of 6.78 ml bidistilled water and 0.52 ml nitric acid (65 wt%) in 30 ml methanol. The latter was added to the TBOT solution in a closed, initially nitrogen flushed system under vigorous stirring. The as-prepared, translucent gels were aged for 4 h to increase the rigidity of the gel network by successive polycondensation reactions. After this first ageing process the corresponding titania gels were redispersed with various amounts of methanol (Table 1) and homogenized for 10 min under vigorous stirring. An opaque, easily stirrable solution resulted. Thereafter the Pt precursor solution (Table 1) was added with a syringe and a second ageing-step for 19 h under vigorous stirring followed. In the case of Pt2NP the introduction of the aqueous $(NH_4)_2PtCl_6$ solution caused an immediate gelation of the sol–gel sample. Hence, it was necessary to add an additional amount of 100 ml methanol to obtain a stirrable solution again.

TABLE 1

Compositions of the Platinum Precursor Solutions, Amount of Methanol (MeOH) Used for the Redispersion of the Titania Gels, and Extra Amount of MeOH Added for the Supercritical Drying

Aerogel	Precursor (mg)	Solvent composition (ml)	MeOH for redispersion (ml)	Extra MeOH for SCD (ml)
Pt2PC	$PtCl_4$ (265)	H_2O (1.8)/MeOH (24)	71	130
Pt2PA	$Pt(acac)_2$ (309)	MeOH (95)	50	80
Pt2NP	$(NH_4)_2PtCl_6$ (349)	H_2O (50)	50 + 100	25
Pt5PC	$PtCl_4$ (683)	H_2O (7)/MeOH (24)	71	130

With Pt2PC, Pt2NP, and Pt5PC orange translucent solutions developed, and in the case of Pt2PA a yellow translucent solution developed. This was highly viscous in the case of Pt2NP.

To exceed the critical state without formation of a vapour–liquid interface inside the pores (10), the sol–gel product as described above was transferred in a Pyrex-glass liner into a net 1.09-liter autoclave together with the appropriate amount of additional methanol (Table 1) to give ca. 375 ml in all cases, thus surpassing the critical volume of the mixed solvent. The corresponding critical data for methanol, as the dominating component of all four SSG solvents used here, are V_c = 118 ml mol^{-1}, T_c = 513 K, and p_c = 8.1 MPa (30). The high-pressure system was flushed with nitrogen, hermetically closed, pressurized to 5 MPa, and heated with a temperature ramp of 1 K min^{-1} to 533 K. The autoclave was kept at the final temperature for 30 min to ensure complete thermal equilibration. The final pressure was about 18 MPa (Pt2PC, Pt2PA) or about 20 MPa (Pt2NP, Pt5PC; with higher water contents). The pressure was then isothermally released at a rate of 0.1 MPa min^{-1}. The system was thereafter flushed with nitrogen and allowed to cool to ambient temperature. Finally the grey aerogel clumps were ground in a mortar. As shown in Table 1, the precursor solution of Pt2NP contained 50 ml water (T_c = 647 K (31)), which can no longer be assumed to be negligible with respect to the SCD temperature. Interpolation via a linear T_c-versus-composition law afforded a SCD end temperature of 553 K.

Portions of the untreated (raw) aerogel powders were pretreated under various conditions in a U-tube reactor. The temperatures given correspond to the oven temperature. GHSV amounted to 1000–2000 h^{-1} (1–2 g aerogel sample). The flows of any gases used were usually adjusted to 0.5 liter min^{-1}. All aerogel samples calcined in air were first treated in a purified nitrogen flow at 573 K for 1 h. After cooling to about 353 K in nitrogen and heating again at 5 K min^{-1}, this time in air, the portions of the raw aerogels were calcined for another 5 h at 573 or 673 K, this being the standard calcination procedure for all the aerogels. Two portions of Pt2PC were at first treated in a similar manner to the standard air pretreatment at 573 K, but at the end of the air procedure a nitrogen step of half an hour was added, followed by cooling to ambient temperature, also in nitrogen. The samples were then heated in flowing hydrogen at 5 K min^{-1} and kept for 3 h at 573 and 673 K, respectively. For another two portions of Pt2PC the temperature was increased at 2.5 K min^{-1} in flowing nitrogen and kept at 373 K for 1 h. After cooling to about 313 K in nitrogen and heating at 2.5 K min^{-1}, this time in hydrogen, these aerogel samples were reduced for another 5 h at 473 and 673 K, respectively. At the end of all hydrogen pretreatments samples were exposed to nitrogen for half an hour at the reducing temperature, followed by cooling to ambient temperature in nitrogen.

The metal loading was generally calculated on the basis of the nominal amounts used (Table 1) and the assumption of a complete reduction of the Pt precursors. The nominal metal loadings were independently confirmed by ICPAES analysis. The assumption of the complete reduction is justified on the basis of recently published data (32, 33) concerning the preparation of Pt sols in refluxing methanol (338 K and ambient pressure). Note that we used 533 K and methanolic pressure larger than ca. 11 MPa.

Nitrogen Physisorption

The specific surface areas (S_{BET}), mean cylindrical pore diameters ($\langle d_p \rangle$), and specific adsorption pore volumes (V_{pN_2}) were obtained from nitrogen physisorption at 77 K using a Micromeritics ASAP 2000. Prior to measurement, all samples were degassed to 0.1 Pa at 423–473 K. BET areas were calculated in a relative pressure range 0.05 to 0.2 assuming a cross-sectional area of 0.162 nm^2 for the nitrogen molecule. The pore size distributions were calculated applying the Barrett–Joyner–Halenda method (34) to the desorption branches of the isotherms (35). The assessments of microporosity were made from *t*-plot constructions, using the Harkins–Jura correlation (36).

X-Ray Diffraction

X-ray powder diffraction (XRD) patterns were measured on a Siemens Θ/Θ D5000 powder X-ray diffractometer. The diffractograms were recorded with detector-sided Ni-filtered Cu$K\alpha$ radiation over a 2Θ-range of 20 to 80° and a position sensitive detector. The mean crystallite sizes were determined from the Scherrer equation (37) at the {101}- or {200}-peak for anatase (38) and the {111}-peak for Pt (39).

Transmission Electron Microscopy

Samples for transmission electron microscopy (TEM) were loaded dry onto perforated, thin carbon films supported on copper grids, aerogel powder being poured onto the carbon film and shaken off five times.

Diffraction-contrast TEM was performed using a Hitachi H-600 operated at 100 kV, with a point resolution of about 0.5 nm. The instrumental magnification had previously been calibrated using the phase constrast from catalase crystals. High-resolution, phase-contrast TEM was carried out on a Philips CM30ST at 300 kV, with a point resolution of 0.19 nm. Here the 0.352-nm lattice fringes from anatase were employed as an internal calibrant of the magnification. Particles were measured from photographic enlargements of the micrographs using a graduated magnifying glass to estimate the equivalent-

circle diameter of the particle image. Only species imaged at just under Gaussian focus were incorporated in the particle size distributions, there often being a distribution of heights and thus defocus conditions within a micrograph. Identification of the Pt component used the usually greater contrast of Pt in comparison to the less electron-dense titania, as well as the rounder, smoother profiles of the metal particles. Images from pure titania aerogels prepared by a similar method were used for comparison. Here the pure titania was prepared following the above-mentioned preparation process (29) with 95 ml methanol for the redispersion step.

The most important parameters obtained from the size distributions were the mean diameter from the volume-weighted distribution, $\langle d \rangle_v$, defined in Eq. [3], and the mean diameter from the surface-area-weighted particle size data, $\langle d \rangle_a$, defined in Eq. (4).

$$\langle d \rangle_v = \sum_i (n_i d_i^4) \Big/ \sum_i (n_i d_i^3) \qquad [3]$$

$$\langle d \rangle_a = \sum_i (n_i d_i^3) \Big/ \sum_i (n_i d_i^2). \qquad [4]$$

$\langle d \rangle_v$ is most appropriate for comparisons with crystallite sizes determined from XRD line broadening, whereas $\langle d \rangle_a$ is used for surface-area studies. The number of Pt particles measured varied from 27 in the case of a coarse sample to 407 for a fine dispersion of Pt, being in the majority of cases over 100. Particle size distributions were obtained in all cases from a range of micrographs representing different areas of the sample grid, and results of the averages were compared between micrographs. The breadth of the size distributions was expressed by the coefficient of variation, the root-mean-square (standard) deviation of diameters from the (unweighted) mean expressed as a (percent) fraction of this mean.

Hydrogen Chemisorption

Hydrogen chemisorption was measured in an all-glass system connected to an oil diffusion pump. The hydrogen used was of 99.999 vol.% purity. About 1 g sample was first evacuated at 423 K (Pt2PC sample reduced at 473 K, reference catalyst) and 473 K (Pt2PC sample reduced at 673 K), respectively for 4 h and then reduced in flowing hydrogen (40 ml min^{-1}) at 463 K, 473 K, and 663 K for 3 h, respectively. Afterwords the samples were degassed at 423 K (low-temperature reduced Pt2PC portion and reference) and 473 K (high-temperature reduced Pt2PC portion) overnight. Adsorption was carried out in the range 296 ± 1 K starting with initial pressures of about 5×10^3 Pa, which were allowed to equilibrate for 2.5 h. After the first isotherm had been recorded, the samples were evacuated down to 10^{-3} Pa during 1 h and the pure physisorption isotherm was measured. The linear region chosen for the zero pressure extrapolation of the chemisorbed amount of hydrogen lay between 10^4 and 3×10^4 Pa.

Thermal Analysis

TG and DTA investigations were performed on a Netzsch STA 409 coupled with a Balzers QMG 420 quadrupole mass spectrometer, equipped with Pt–Rh thermocouples and using Pt crucibles, a heating rate of 10 K min^{-1}, and an air flow of 25 ml min^{-1}. The sample weight was about 20 mg and the α-Al_2O_3 reference weight 62.5 mg.

Total carbon and hydrogen contents were determined with a LECO CHN-900 elemental microanalysis apparatus.

Catalytic Characterization

The reactions were performed in a 200-ml, flat-bottomed glass batch reactor (D = 75 mm) equipped with gas inlet and outlet, condenser, thermometer, and magnetic stirrer. The stirring speed was 1500 rpm and the length of the magnetic rod 50 mm. The reaction temperatures were set at 303 K (*trans*-stilbene, TS) and 343 K (benzophenone, BP). As solvents, *i*-propylacetate and butylacetate were used, respectively. The flow rates were measured by a rotameter. At first 15–20 mg of catalyst powder (<250 μm) was suspended in 30 ml solvent and the batch system was flushed with nitrogen for 2 min. Thereafter the aerogel was prehydrogenated with an increased hydrogen flow (140 ml min^{-1}). After 15 min the hydrogen flow was reduced to 30 ml min^{-1} (atmospheric pressure) and 2 mmol reactant in 10 ml solvent was injected. Samples of the reaction mixture (ca. 0.5 ml) were periodically taken, filtered, and analyzed by gas chromatography.

A HP 5890A type gas chromatograph, equipped with a HP 7673A automatic injector and a flame ionization detector, was used. The separating column was a 30 m × 0.53 mm × 1.33 μm HP-20M carbowax wide pore capillary column, operated between 373 and 493 K, with a helium carrier gas flow rate of 40 ml min^{-1} and a split ratio of 13.

To minimize the influence of side reactions, the initial rates were determined from reactant consumptions below 5% conversion. Preliminary tests, in which the amount of catalyst and the stirring speed were varied within a wide range, showed that the reaction rate in [mol/s/g_{Pt}] was independent both of the amount of catalyst (≤50 mg) and of the stirring speed (≥500 rpm), indicating that interparticle mass transfer limitation could be ruled out. For a few of the most active catalysts the experimental errors of the catalytic testing were determined, estimated

from three consecutive measurements. They ranged between 6 and 8%. Due to the lack of any commercial Pt/titania catalyst, a 5 wt.% Pt/alumina catalyst from Engelhard (E 7004) has been chosen as a reference.

RESULTS

The morphological and textural properties of the Pt–titania aerogels are listed in Table 2.

Nitrogen Physisorption

It is known that one has to be fairly cautious interpreting absolute physisorption data derived from such highly structured aerogels (40). Usually total specific pore volumes (V_{pN_2}) measured are too low compared with the appropriate bulk densities. Obviously the largest pores, which contribute most to V_{pN_2}, remain undetected by nitrogen physisorption. Nevertheless, comparisons within a preparation series of such materials are still meaningful.

All aerogels showed a type IV isotherm with a type H1 desorption hysteresis according to IUPAC classification (41). Pore size distributions derived from the desorption branch (35) are illustrated in Fig. 1 for the Pt5PC sample, calcined in air at 573 K, as a representative of the whole Pt2PC, Pt2PA, and Pt5PC series, and for a Pt2NP portion also calcined in air at 573 K, as a representative of the Pt2NP series. They all show pronounced meso- to macroporosity with only little microporosity and specific micropore surface areas estimated from the corresponding *t*-plot analysis of up to 14 $m^2 g^{-1}$.

Moreover, it clearly emerges from Table 2 that the textural properties are virtually independent of the pretreatment medium used and temperature up to 673 K. With respect to the temperature chosen, however, one observes a slight, consistent decrease in S_{BET} and V_{pN_2} lying within the precision range of the physisorption measurements themselves. Aerogel materials with low water content (Pt2PC, Pt2PA; Table 1) have S_{BET} of 167 to 184 $m^2 g^1$, V_{pN_2} of 0.69 to 0.85 $cm^3 g^{-1}$, and very broad, asymmetric pore size distributions (Fig. 1). The latter also emerges from the comparison of the graphically determined pore size maxima (ca. 50 nm) with the mean cylindrical pore sizes $\langle d_p \rangle$ given in Table 2. In contrast to this, the high water content aerogels Pt5PC and Pt2NP show a significant decline in S_{BET} to about 150 $m^2 g^{-1}$ and a

TABLE 2

Morphological and Textural Properties of the Platinum–Titania Catalysts Pretreated in Air and/or Hydrogen at Various Temperatures

Aerogel	Pretreatment (K)		S_{BET} (S_t) (m^2/g)[a]	$\langle d_p \rangle$ (nm)[b]	V_{pN_2} (cm^3/g)	Crystallinity and $\langle d_c \rangle$ (nm)[c]	$\langle d \rangle_v$ (nm)[d]
	Air	Hydrogen					
Pt2PC	—	—	—	—	—	A/Pts 8.0/—	3.8
	573	—	184(13)	17(50)	0.80	A/Pts 8.2/—	3.8
	673	—	176(14)	16(45)	0.69	A/Pts 8.1/—	—
	573	573	184(13)	16(50)	0.75	A/Pts 7.9/—	3.6
	573	673	178(14)	16(45)	0.69	A/Pts 7.9/—	3.6
	—	473	182(9)	18(50)	0.80	A/Pts 8.0/—	3.8
	—	673	175(12)	19(55)	0.85	A/Pts 8.2/—	3.9
Pt2PA	—	—	—	—	—	A/Pt 7.5/17.5	68
	573	—	169(10)	18(50)	0.75	A/Pt 7.6/19.1	34
	673	—	167(11)	17(50)	0.71	A/Pt 7.6/17.9	—
Pt2NP	—	—	—	—	—	A/Pts 8.7/—	4.4
	573	—	147(10)	30(30)	1.11	A/Pts 8.7/—	—
	673	—	147(2)	30(30)	1.13	A/Pts 8.7/—	—
Pt5PC	—	—	—	—	—	A/Pts 9.1/—	4.1
	573	—	150(9)	29(45)	1.06	A/Pts 9.1/—	—
	673	—	147(9)	26(50)	0.97	A/Pts 9.3/—	—

[a] (S_t), in parentheses, denotes specific micropore area derived from *t*-plot analysis.

[b] $\langle d_p \rangle = 4V_{pN_2}/S_{BET}$; numbers in parentheses denote graphically determined pore size maxima.

[c] A, anatase; Pts, platinum shoulders; $\langle d_c \rangle$ mean crystallite sizes of anatase and/or platinum derived from XRD line broadening. (—, not determinable)

[d] $\langle d \rangle_v$, volume-weighted-mean particle sizes derived from TEM.

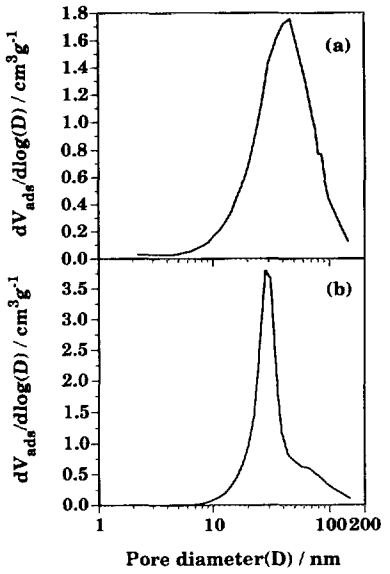

FIG. 1. Differential pore size distributions derived from the desorption branch of nitrogen physisorption. (a) Pt5PC calcined in air at 573 K; (b) Pt2NP calcined in air at 573 K.

comparable increase in V_{pN_2} to about 1.1 $cm^3 g^{-1}$. Besides, with Pt2NP the 50 ml extra water, added via the precursor solution, caused narrower and virtually symmetric pore size distributions (Fig. 1). Also, a more pronounced parallelism of the hysteresis branches developed at lower relative pressures, such an effect often corresponding to narrower pore size distributions (41). This is likely a result of the increased water reactivity under the conditions applied during high-temperature SCD. On a molecular scale water can cause dissolution, reprecipitation, depolymerization, repolymerization, alkoxylation, and enhanced syneresis (network densification) leading to crystallographic and chemical and/or restructuring phenomena in such materials. Such processes include some Ostwald ripening, coalescence coarsening/sintering, and syneresis resulting in lower surface areas and larger pore volumes.

X-Ray Diffraction

Figure 2 depicts the X-ray patterns of the raw aerogels. The crystalline fractions are in general made up of Pt crystallites (39) and well-developed anatase crystallites (38). The mean anatase crystallite sizes range from 7.5 to 9.3 nm slightly increasing with increasing water content (Table 2), allowing for enhanced crystallinity of the anatase domain due to the marked reactivity of water under such conditions. Pt2PC, Pt2NP, and Pt5PC show broad Pt shoulders mainly disguised by the anatase pattern. However, Pt2PA derived from $Pt(acac)_2$ consists of well-developed Pt crystallites of about 19 nm mean size.

Moreover, Table 2 clearly illustrates that the crystallinity of both anatase and Pt are virtually independent of the pretreatment medium used and temperature up to 673 K.

Transmission Electron Microscopy

In Fig. 3, we see a representative diffraction-contrast TEM image from a pure titania aerogel synthesized in a similar manner to the binary Pt–titania systems, together with an image from raw Pt5PC. The small round dark contrast features present in the latter case and not in the former are assumed to be the Pt crystallites indicated from X-ray diffraction analysis. Support for this is provided by high-resolution TEM micrographs of the Pt2PC sample calcined in air at 573 K (Fig. 4), where a proportion of

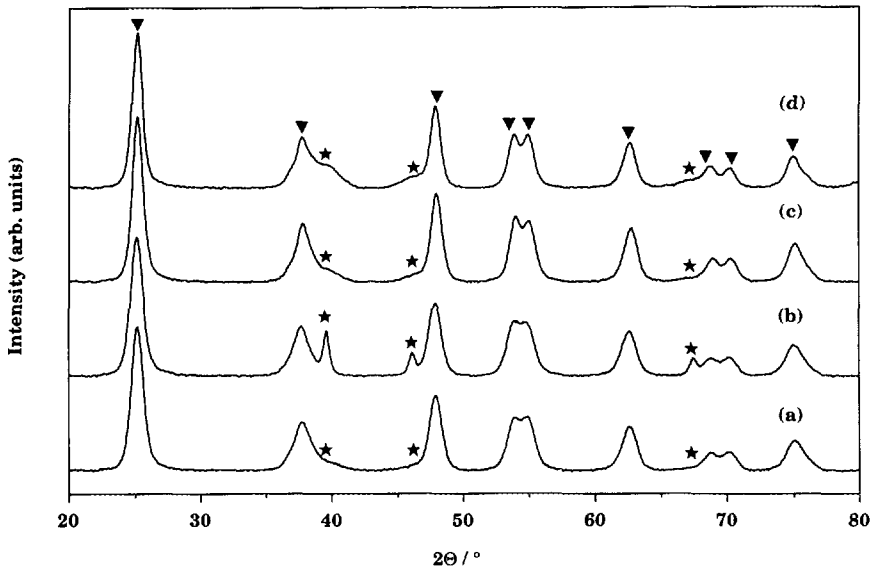

FIG. 2. X-ray diffraction patterns (Cu$K\alpha$) of the new aerogels. (a) Pt2PC; (b) Pt2PA; (c) Pt2NP; (d) Pt5PC; (▼) anatase; (★) platinum.

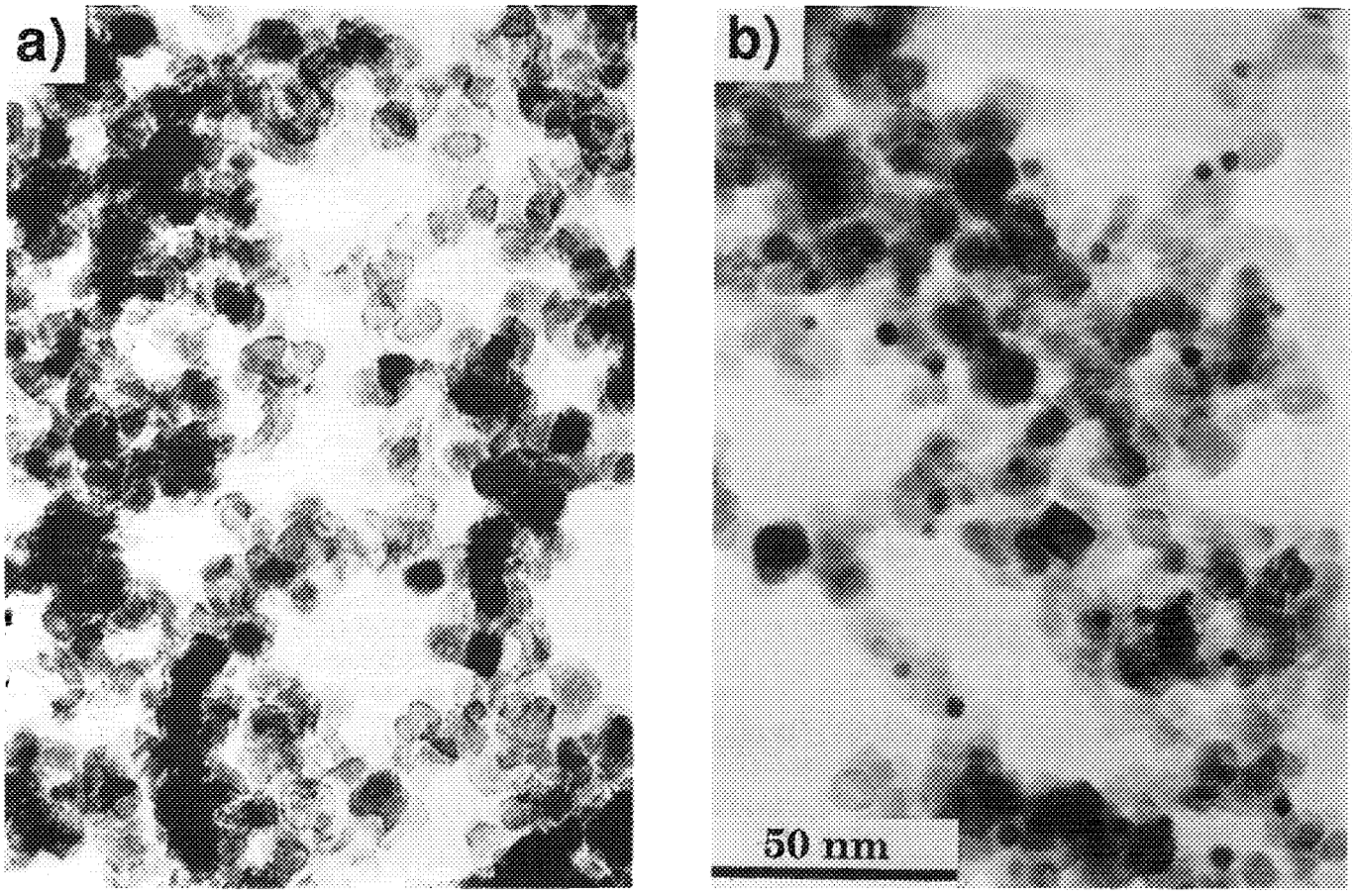

FIG. 3. Diffraction-contrast TEM images. (a) Pure titania similarly prepared as the binary aerogels, calcined in air at 573 K; (b) raw Pt5PC.

the dark contrast features contained the characteristic 0.227-nm {111}, and rarely 0.196-nm {200}, lattice fringe spacings of elemental Pt. The other similar contrast features present in the high-resolution micrographs of Pt2PC (but not in those of pure titania aerogel) are probably, on the grounds of contrast and shape, Pt species which happen to be at the wrong orientation or defocus/height (or possibly too fluxional under beam "heating" effects (42)) to show phase contrast. Comparison of the particle size distribution for the Pt2PC catalyst, calcined in air at 573 K, measured from diffraction-contrast micrographs with that measured from high-resolution images containing Pt fringes, showed good agreement, although the size distribution of "fringed" particles is a little narrower. If the other small, round, highly contrasting particles visible in the high-resolution micrographs, not showing phase contrast, are added to the distribution data then even better agreement between diffraction-contrast TEM and phase-contrast TEM size distributions is obtained.

From the high-resolution images (Fig. 4), we see that the small particles of the Pt2PC sample, calcined in air at 573 K, are mostly monocrystalline (fcc) or singly twinned (42). However, in the case of Pt2PA, the aerogel prepared with $Pt(acac)_2$ as Pt precursor, more irregular shapes and internal contrasts seen in the diffraction-contrast TEM images indicate a greater degree of polycrystallinity than is the case with aerogels Pt2PC, Pt2NP, and Pt5PC. This is as suggested by a comparison of XRD-determined mean crystallite sizes (18 nm, 19 nm) and volume-weighted particle sizes obtained from TEM (68 nm, 34 nm) for the raw Pt2PA and the portion of Pt2PA calcined in air at 573 K, respectively (Table 2). Moreover, the absence of strongly anisotropic particle profiles (long, thin, or ellipsoidal) of either Pt (in the well-dispersed aerogels) or titania (in general) in the micrographs shows that the particle shapes must also be relatively isotropic (e.g., near-spherical or cubic) in three dimensions, there being no preferred orientation with respect to the electron beam in these samples. Comparison of Pt particle size data between micrographs gave in general good agreement. This correspondence was best when the sample size was high: for example, in the case of one sample of 407 particles, all the mean diameters obtained from separate micrographs of between 33 and 80 particles lay within $\pm 5\%$ of the overall mean, the calcu-

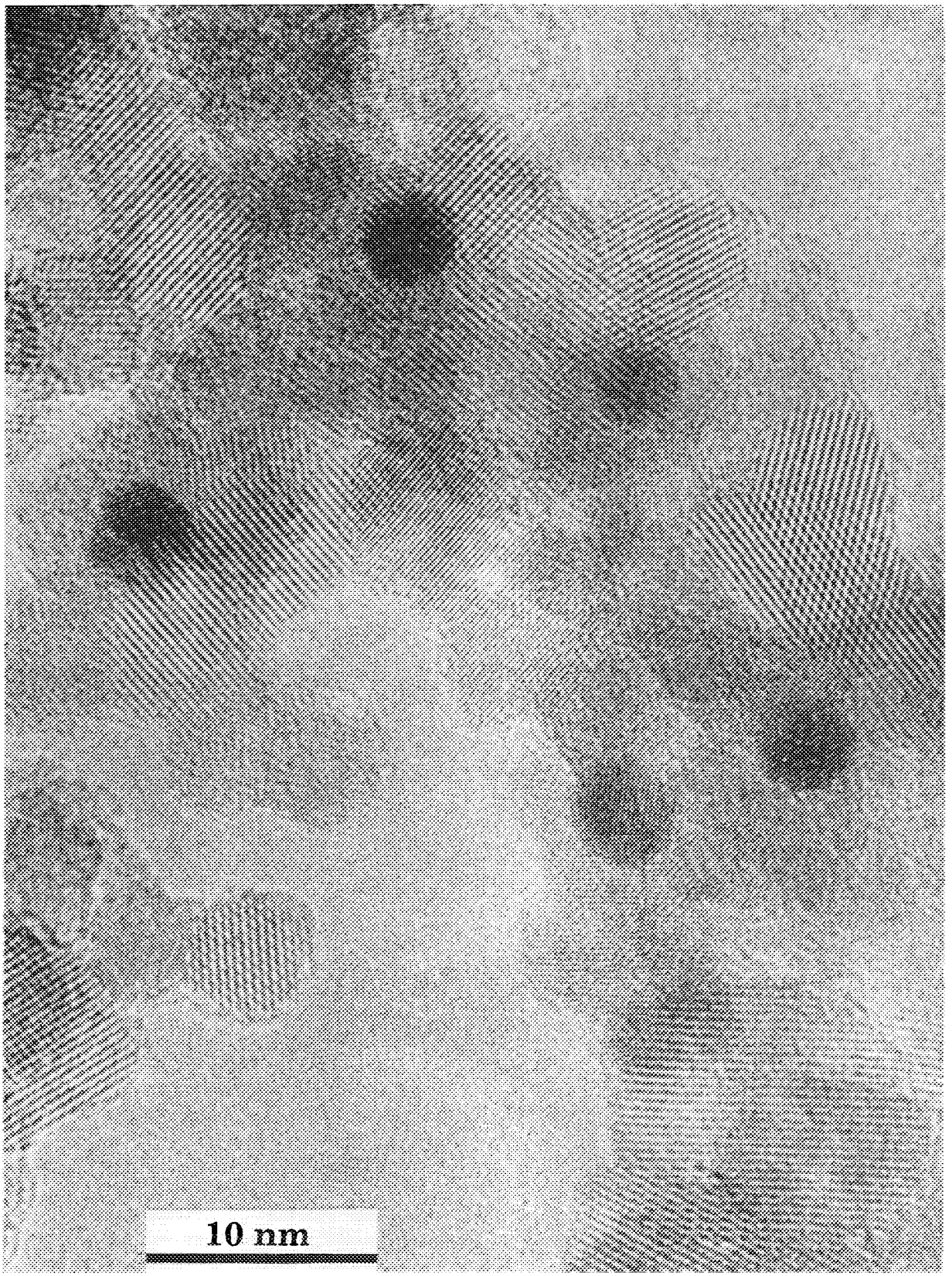

FIG. 4. High-resolution TEM micrograph of sample Pt2PC calcined in air at 573 K.

lated 95%-confidence limits being consistent with deviations caused by statistical sampling error from a homogeneous population (43).

The size distribution data from the diffraction-contrast TEM micrographs of the raw samples are shown in Fig. 5. In agreement with XRD line-broadening experiments, the TEM data show that good dispersions are achieved with the precursors $PtCl_4$ at 2 and 5 wt.%, as well as with $(NH_4)_2PtCl_6$ at 2 wt.%. Here the majority of particles have diameters smaller than those of the anatase crystallites, whereas for the aerogel prepared with $Pt(acac)_2$ as precursor the Pt particles are mostly larger than the titania species.

Most of the aerogel samples examined (Pt2PC, Pt2NP, Pt5PC) were monomodal in size distributions. In contrast, Pt2PA, the aerogel prepared from a $Pt(acac)_2$ precursor, had modes at around 30 and 100 nm, as well as possibly at about 10 nm (not distinguished with certainty from anatase). The coefficients of variation for all single-mode particle size distributions, as well as for the single mode from the multimodal size data for raw Pt2PA, lay between 14 and 21%.

Figure 6 shows size distributions for portions of Pt2PC both raw and following the various pretreatments in air and/or hydrogen. We see no significant change or evidence of sintering, despite the small Pt particle size, which confirms the results from XRD. Neither was obvious change on calcination observed in the actual size distribution of the raw Pt2PA, despite the widely differing values for $\langle d \rangle_v$ presented in Table 2. This anomaly is due to two particles from the larger mode being present on the micrographs of the raw sample, but statistically absent in the images of the calcined material.

More qualitatively TEM data confirmed that the structure of the titania aerogels was hardly changed by the presence of varying Pt precursor solutions in the sol–gel–aerogel preparation and the applied pretreatment (Fig. 3). Primary particle diameters lie between 5 and 11 nm in every case being in good agreement with the corresponding mean crystallite sizes derived from XRD.

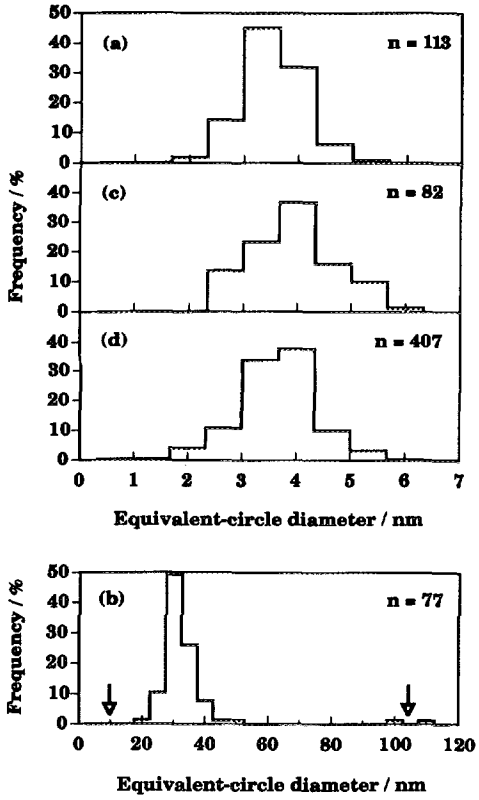

FIG. 5. Particle size distributions derived from TEM for the raw samples. (a) Pt2PC; (b) Pt2PA; (c) Pt2NP; (d) Pt5PC. *n* represents the number of platinum particles measured. Arrows in (b) represent the positions of apparent further modes in the size distribution.

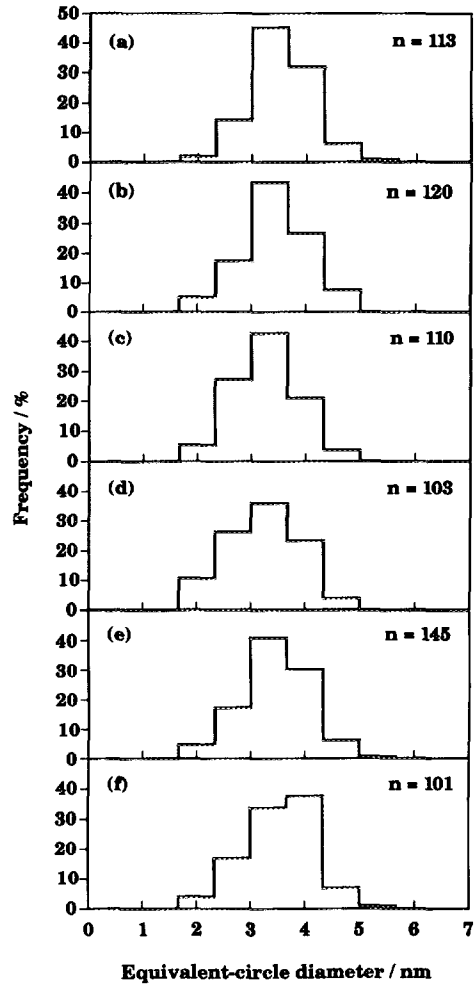

FIG. 6. Particle size distributions derived from TEM for Pt2PC catalysts treated in air and/or hydrogen at different temperatures. (a) Raw; (b) air at 573 K; (c) air at 573 K followed by hydrogen at 573 K; (d) air at 573 K followed by hydrogen at 673 K; (e) hydrogen at 473 K; (f) hydrogen at 673 K. *n* represents the number of platinum particles measured.

In summary, the TEM images demonstrate a remarkable homogeneity, reinforcing the reliability of the measurements. The error on the mean particle sizes may amount to 10–20% in the case of monomodal particle size distributions, and much higher in the case of multimodal distributions. For all aerogel catalysts derived from chloridic Pt precursors one can conclude in general that the monomodal preparations are strikingly monodisperse and homogeneous in the context of metal dispersions and conventionally prepared heterogeneous catalysts and show a remarkable chemical and thermal stability (Table 3, Fig. 6).

Hydrogen Chemisorption

In our case we considered it to be of rather doubtful value to derive dispersity information and thus eventual turnover frequencies from chemisorption measurements of raw, carbon-covered aerogels or aerogel samples oxidatively pretreated in air, as they were catalytically tested without any prereduction at elevated temperatures. Such pretreatments clearly cause some surface restructuring, surface relaxation, and/or changes in the surface composition. Thus dispersion and eventual turnover frequency data, based on such rather theoretical adsorption studies, would be rather unreliable. It is also obvious, however, that TEM-derived dispersions do not give a direct measure of the catalytically relevant number of the accessible Pt surface fraction either, enabling the calculation of real, intrinsic activities. In the special case of our aerogel samples, we mainly deal with fairly smooth and round particle profiles and narrow size distributions, favouring the TEM-derived size data for information on dispersion.

As a consequence of the described uncertainty in the determination of the accessible Pt surface atoms we com pare the reaction rates based on the metal content.

Hydrogen chemisorption with the two Pt2PC samples, one hydrogen pretreated at 473 K, the other at 673 K, resulted in dispersion values of 13 and 7%, respectively, exhibiting a significant decrease in hydrogen chemisorption capacity with increasing reduction temperature (27, 28). The dispersion of the Engelhard catalyst amounted to 15%.

Thermal Analysis

Thermal analysis was performed in flowing air for a series of both raw and variously pretreated Pt2PC samples. Figure 7 depicts the thermoanalytical results measured for the raw aerogel Pt2PC. The weight losses origi-

TABLE 3

Liquid-Phase Hydrogenation at Ambient Hydrogen Pressure of *trans*-Stilbene at 303 K and Benzophenone at 343 K

Aerogel	Pretreatment (K)		$\langle d \rangle^a$ (nm)	$r_0 \times 10^5$ (mol/s/g_{Pt})	
	Air	Hydrogen		*trans*-Stilbene	Benzophenone
Pt2PC	—	—	3.7	7.0	29.4
	573	—	3.7	10.7	32.7
	673	—	—	10.0	32.7
	573	573	3.5	6.9	21.4
	573	673	3.5	5.2	19.5
	—	473	3.7	5.7	21.2
	—	673	3.8	1.2	2.4
Pt2PA	—	—	49	0.2	0
	573	—	34	0.4	0
	673	—	—	0.2	—
Pt2NP	—	—	4.2	8.0	23.5
	573	—	—	7.4	—
	673	—	—	8.0	26.2
Pt5PC	—	—	3.9	7.7	29.2
	573	—	—	9.5	—
	673	—	—	9.2	32.5
5% Pt/Al_2O_3			4.4	5.5	15.8

Note. Initial rates (r_0) and area-weighted-mean particle sizes ($\langle d \rangle_a$) are shown.

[a] Derived from TEM analysis (see Experimental section).

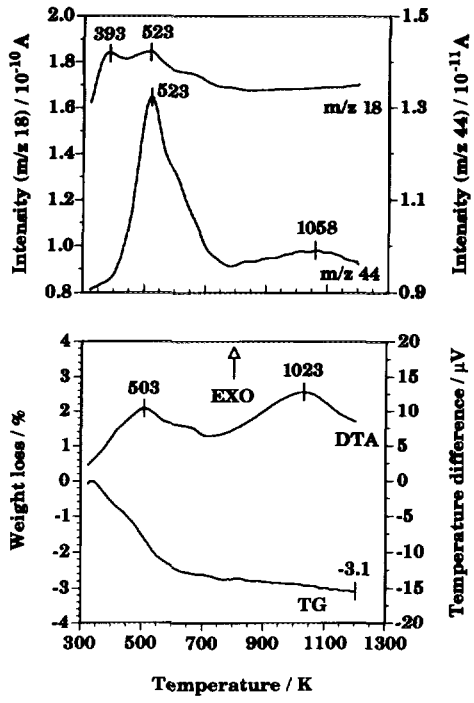

FIG. 7. Thermoanalytical results of the raw aerogel Pt2PC monitored in air. Bottom: TG and DTA profiles; top: mass/charge ratios (m/z) of $m/z(CO_2^+)$ = 44 (CO_2) and $m/z(H_2O^+)$ = 18 (water).

nate from the oxidation of organic residues and predominantly from the evolution of water (desorption of physisorbed water, dehydroxylation). This conclusion clearly emerges from relating the TG profile with the monitored mass/charge ratios (m/z) $m/z(CO_2^+)$ = 44 (CO_2) and $m/z(H_2O^+)$ = 18 (water) (Fig. 7). The weight losses of all samples studied, determined up to 1173 K, are compared in Fig. 8, distinctly reflecting the influence of the applied pretreatment temperature. Based on a comparison of the amounts of water and CO_2 released from the Pt2PC samples, it is evident that the dominance of the evolved-water contribution to the overall weight loss increases with increasing pretreatment temperature. This is due to the marked similarity of water evolutions for both the raw and the variously pretreated Pt2PC catalysts together with the significantly decreasing amount of organic residues with increasing pretreatment temperature, as shown in Fig. 9. The liberation of water, representatively displayed in Fig. 7, began with all samples at room temperature and exhibited maxima at about 393 and 523 K. The weight loss at the beginning originates mainly from physisorbed water but later on is dominated by the contribution of water from oxidation of the organics. As mentioned, a distinct decline of the organic contents, reflected by decreasing intensities of the CO_2 traces, is seen after any thermal pretreatments up to 673 K, and the extent of this decrease is in fact virtually independent of the pretreatment medium (air or hydrogen) used, as illustrated in Fig. 9. Two steps of CO_2 evolution could be detected for the whole Pt2PC series examined. The first step of CO_2 evolution started at ca. 410 K and attained a maximum at about 523 K. From about 790 K a second production of CO_2 occurred reaching its maximum at approximately 1058 K. In accordance with this, the DTA curves are dominated by two broad exothermal peaks at about 503 and 1023 K related to the corresponding oxidation of organic residues and subsequent formation of CO_2 (Fig. 7).

Thus thermal analysis clearly indicates that two "kinds" of organic residues exist in the Pt2PC samples.

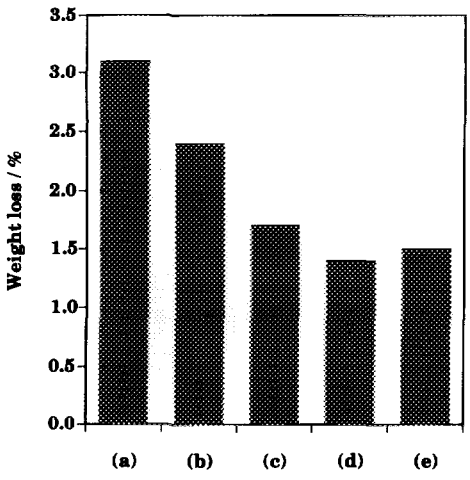

FIG. 8. Thermoanalytical weight losses, determined in air up to 1173 K, of Pt2PC catalysts pretreated in air and/or hydrogen at different temperatures. (a) Raw; (b) air at 573 K; (c) air at 673 K; (d) air at 573 K followed by hydrogen at 673 K; (e) hydrogen at 673 K.

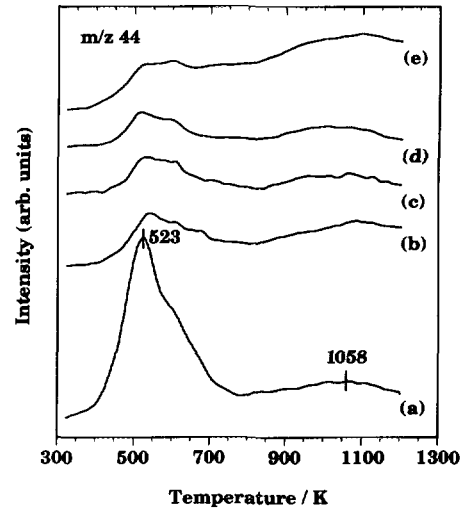

FIG. 9. CO_2 evolution ($m/z(CO_2^+)$ = 44) of Pt2PC catalysts monitored in air, pretreated in air and/or hydrogen at different temperatures. (a) Raw; (b) air at 573 K; (c) air at 673 K; (d) air at 573 K followed by hydrogen at 673 K; (e) hydrogen at 673 K.

The occurrence of these two CO_2 evolutions does not depend on the pretreatment media and temperatures used (Fig. 8). The low-temperature step, dominating the raw sample, stems from organic species mainly covering the accessible surface. A part of this low-temperature form reveals a high resistance towards pretreatments up to 673 K in air and/or hydrogen. This can be attributed to organic residues sitting deep inside the porous titania matrix. Their removal could thus be diffusion controlled. The high-temperature CO_2 evolution, arising at about 790 K and being thermoanalytically quite stable, could be assigned to organics being incorporated within the titania matrix and thus scarcely affected by the pretreatment procedures applied.

With raw Pt2NP and Pt5PC, aerogels with high water contents (Table 1), the carbon contents from elemental analysis lay around 0.5 wt.% in the case of raw Pt2PC and Pt2PA, both having low water contents around 0.7 wt.%. The hydrogen contents are fairly equal over all samples (ca. 0.7 wt.%) and represent a superposition of water originating from oxidation and water being either physi- or chemisorbed. The carbon contents show two effects. All aerogels contain a considerable amount of organic residues after high-temperature SCD. This is mainly attributed to the realkoxylation of titanium-bound hydroxyl groups (9, 44). Probably to a low extent some organic oxidation products (precursor reduction) as well as organic species catalytically decomposed on the Pt surface must also be taken into account. The decreased carbon content for the aerogels Pt5PC and Pt2NP can be explained by the extra amount of water in the precursor solutions, leading to some competitive hydroxylation of the oxidic surface.

Hydrogenation Activity

The catalytic behaviour of Pt–titania aerogels in the liquid phase hydrogenation of *trans*-stilbene and benzophenone is summarized in Table 3. Note that the area-weighted-mean particle sizes ($\langle d \rangle_a$) are only used as a relative measure for the dispersion, since accessibility is not taken into account with this value. The initial activities have been calculated on a Pt weight basis (r_0 = [mol/s/g_{Pt}]) with errors of 6–8%. As we have seen above, the aerogel catalysts exhibit a pronounced stability for both the titania matrix and the Pt. Consequently any significant change in specific activity within an aerogel series must be due to some surface structure, composition variation, and/or occlusion variation. The latter points cannot be completely elucidated on the basis of the results obtained in this work.

Even the raw, well-dispersed aerogels, Pt2PC, Pt5PC, and Pt2NP, showed excellent initial activities for *trans*-stilbene and benzophenone hydrogenation, being about 1.5 times higher than that of the commercial reference catalyst. This is despite the fact that these aerogels contain 0.47 to 0.74 wt.% of carbon as organic residues and some chlorine from the Pt precursors. In contrast, Pt2PA derived from $Pt(acac)_2$ is poorly dispersed and had only minor activity referred to the Pt weight.

Taking into account the constancy of the SSG volume for Pt2PC and Pt5PC with the concomitant increase in Pt-precursor concentration and the larger amount of water in the precursor solution for Pt5PC, a comparison of the catalytic data reveals that the significant changes in the aerogel preparation of Pt5PC did not produce any evident changes in the catalytic performance. Thus the formation of the Pt particles seems to be quite tolerant of the SSG preparation with subsequent SCD.

Considering the effects of the thermal pretreatment, two points have to be emphasized. First, there is an unambiguous benefit of the calcination in air at 573 or 673 K. The rise in activity surpassed 50% in the case of Pt2PC, which is likely due to the oxidative removal of a fraction of organic impurities from the Pt surface. It is important to emphasize that the rates of hydrogenation of *trans*-stilbene and benzophenone are influenced qualitatively in the same way, which indicates that the observed catalytic behaviour of these samples is not specific to the reduction of only one type of functional group. Second, the pretreatments in hydrogen caused either mainly detrimental or no effects. The negative influence of the heat pretreatment at 673 K in hydrogen without foregoing calcination in air is very striking: in comparison with the raw sample the initial rates decreased by a factor of 6 and 12.5 in both reactions, while the Pt dispersions as determined by TEM were hardly affected by any of the heat pretreatment procedures. We propose that the contradictory influence of oxidative and reductive pretreatments cannot be assigned only to the transformation of organic residues on the Pt surface. It is very likely that the interaction of the Pt/H_2 system with the titania is responsible for the detrimental effect of the high-temperature hydrogen pretreatments at 673 K (27, 28).

Three of the four aerogels prepared showed markedly higher initial activity in the reduction of C=C and C=O functional groups than that of the commercial, optimized Pt/alumina catalyst. This difference attained 100% in the case of the $PtCl_4$-derived aerogel catalysts. Note that the presented reaction rates for the aerogels, prepared by a direct preparation method, are conservative estimates, since possible inaccessibility of Pt particles has not been taken into account. Concerning the future application of these materials, it is unlikely to exceed 400 K in the presence of hydrogen, which is the typical upper limit of liquid-phase hydrogenations in fine chemistry. In fact, there

seems to be no restriction of their use in oxidation reactions up to 673 K.

DISCUSSION

Structural Aspects

The marked meso- to macroporosity of the aerogel samples, combined with their relatively high thermal stability, renders the materials promising candidates for use as, e.g., liquid-phase catalysts. Wide pores make the large internal surface area highly accessible for reagents, minimizing effects of pore diffusion control, i.e., yielding a high effectiveness factor, η. Although both *trans*-stilbene (0.5 × 1.1 nm) and benzophenone (0.5 × 1.0 nm) are bulky molecules, from the pore size distributions depicted in Fig. 1 we can see that no size exclusion effects should occur (in the case where the Pt particles are located on pore surfaces). With regard to the porosity, it was confirmed that the pore structure is likely to be preserved in solution, since the textural properties after catalytic use and conventional redrying were virtually unchanged.

Making the assumption of a H/Pt_s adsorption ratio of 1, the dispersions estimated from H_2 chemisorption are in all cases lower than TEM-derived values assuming a cubic shape with one face bound to the surface (45). This may be an indication of partial occlusion of the Pt surface fraction by the titania (46) and/or by contaminants arising from the preparation applied and the precursors (carbon-, chlorine- nitrogen-containing species) and/or by TiO_x ($x < 2$) overlayers as suggested in (27, 28) in the case of aerogel samples prereduced at elevated temperatures (673 K). The direct preparation route used for metal and oxidic matrix is likely to lead to some entrapment of Pt particles between anatase crystallites, caused by structural rearrangements occurring between the disordered SSG product and nanocrystalline aerogel stages. Nevertheless, López and co-workers (14–18) claim that they obtained promising catalytic performances, especially with respect to marked deactivation resistance, by intimate mixing of both matrix and metal precursors from the beginning of the SSG preparation. Moreover, preliminary studies in our laboratory have shown that conventional impregnation procedures using preformed aerogel powders did not succeed in improving the catalytic characteristics in comparison with the reference Pt/alumina catalyst.

In the case of aerogels reduced at higher temperatures (673 K), coverage of Pt by TiO_x ($x < 2$) overlayers is possible, as has previously been suggested (27, 28). As both the TEM-derived Pt particle size and the physisorption-derived porosity remain virtually constant when a sample is subjected to reductive pretreatments the marked decline in chemisorption-derived dispersion with reduction temperature is indeed likely to indicate coverage of a part of the Pt surface fraction. However, this decline is not as well marked as it often is in the literature (22, 23, 27, 28).

The low Pt dispersion and high crystallinity of Pt2PA (synthesized from $Pt(acac)_2$) is in marked contrast to those of the other samples prepared from the chloro–platinum complexes. On mixing the Pt salts with the methanolic titania dispersions, the observed colours suggest that the Pt ions remain unreduced at this stage, and thus the metal reduction and particle formation occur during the SCD process. Note that heating hydrogen hexachloroplatinate(IV) with methanol in the presence of water to boiling point at atmospheric pressure, here with organic rather than inorganic polymers, is a known method of forming colloidal Pt(0) (32, 33). Duff *et al.* (32) showed the particles to be metal with the help of EXAFS and high-resolution TEM. The final size distribution of the metal particles will be determined by the balances between the processes of nucleation, autocatalytic reductive growth (42), and homo- and heterocoagulation (32, 47, 48). These will in turn be affected by such factors as the nature of the Pt precursor, pH, concentrations and concentration heterogeneities, steepness of the temperature ramp, extent of binding of the precursor to the support, and the surface charge and mobility of the nascent metal particles. From the present results, it is not yet possible to assign firmly the most important factors influencing the obtained size distributions; it is not even known whether Pt(II)/Pt(IV) reduction kinetics or Pt(0) particle combination processes play the dominant role. Further work is presently underway to elucidate some details of the mechanism of metal particle formation in these systems.

The morphological and textural stability of the titania matrix on the one hand, and the stability of the Pt particles towards sintering on the other, after pretreatments in air and/or hydrogen at various temperatures up to 673 K, are essential properties of our Pt–titania aerogel catalysts. Applications in liquid phase catalysis cause a refilling of the porous titania structure, creating differential capillary forces. The resulting shearing forces have to be sustained by the tenuous aerogel skeleton. Nevertheless, with future high-temperature applications in mind, we have obviously succeeded in preparing aerogel catalysts thermally stable up to 673 K, the highest temperature investigated. This stability justifies the creation of a large, internal surface area of high accessibility.

Catalytic Aspects

A striking effect of the different Pt precursor solutions is clearly the marked difference in the platinum particle size distribution (Fig. 5, Table 3) between chloride-derived (Pt2PC, Pt2NP, Pt5PC) and acetylacetonate-derived Pt–titania aerogels (Pt2PA). The well-dispersed, raw aerogels (Pt2PC, Pt2NP, Pt5PC) exhibit high initial rates

actually superior to those of the commercial reference catalyst. This catalytic performance is remarkable, considering the relatively high impurity levels consisting of 0.47 to 0.74 wt.% carbon in addition to chlorine in Pt2PC, Pt2NP, and Pt5PC, as well as nitrogen in Pt2NP. We can conclude thus that a considerable fraction of the active surface sites must already be available in the raw aerogel catalysts.

The consecutive oxidative pretreatments at 573 K or above showed either significantly promoting or no effects on the specific activities. In contrast, all hydrogen pretreatments carried out with portions of Pt2PC caused either mainly inhibiting or no effects on the specific activities. Considering the constancy of the Pt particle size within the Pt2PC series, it emerges that the catalytic effects within an aerogel series must be dominated by some varying contamination or inactivation of part of the Pt surface fraction. So, within the pretreatment series particle size influences can virtually be ruled out.

From thermal analysis it emerges that thermal pretreatment in air or in hydrogen removes a significant amount of the organic residues. These studies provide only some integral information, chiefly dominated by the contribution of the oxidic matrix. Besides carbon, the Pt2PC, Pt2NP, and Pt5PC catalysts contain chlorine originating from the Pt precursors used. Kim *et al.* (49) showed that calcination in air removes only part of the chlorine in the Pt surface layers up to 673 K. However, reduction in hydrogen removes virtually all chlorine from the surface layers up to 473 K. It is known that superficial chloride species should be able to promote hydrogenation of carbonyl groups in the presence of atomic hydrogen provided by the neighbouring Pt sites. However, Wieckowski (50) studied the potential dependence of the adsorption of labelled chloride on a freshly prepared Pt/Pt electrode and revealed that up to 100 mV (versus reversible hydrogen electrode) only negligible adsorption occurred. This range corresponds to the electrochemical potential usually pertaining to liquid-phase hydrogenations. So, under such conditions surface chloride is expected to be displaced by the adsorption of hydrogen. We can thus conclude that in our work chlorine contaminants may play a role but cannot be responsible for the whole effect on hydrogenation activity caused by reductive pretreatments. In general, an oxidative pretreatment at temperatures higher than 573 K leads to some significant purification of the Pt surface. In the case of the hydrogen pretreatments the removal of the organics seems to be compensated, especially at elevated temperatures (>473 K), by the partial coverage of the Pt surface fraction with TiO_x overlayers (27, 28) shown by the suppressed hydrogen chemisorption capacity measured for the high-temperature reduced aerogel catalyst (673 K).

In summary, the present studies demonstrate that high-surface-area Pt–titania aerogels with marked meso- to macroporosity can be synthesized by high-temperature SCD. Both the Pt particles and the titania matrix possess a remarkable structural stability up to 673 K. Varying the Pt precursor solution, different Pt particle size distributions can be obtained. The well-dispersed Pt–titania aerogels, derived from chloridic Pt precursors, show excellent hydrogenation activity in comparison with a commercial reference catalyst.

REFERENCES

1. Kistler, S. S., *Nature* **127,** 741 (1931).
2. Kistler, S. S., and Swann, S., *Ind. Eng. Chem.* **26,** 388 (1934).
3. Nicolaon, G. A., and Teichner, S. J., *Bull. Soc. Chim. Fr.*, 1906 (1968).
4. Vicarini, M. A., Nicolaon, G. A., and Teichner, S. J., *Bull. Soc. Chim. Fr.*, 1466 (1969).
5. Vicarini, M. A., Nicolaon, G. A., and Teichner, S. J., *Bull. Soc. Chim. Fr.*, 1651 (1970).
6. Pajonk, G. M., *Appl. Catal.* **72,** 217 (1991).
7. Ko, E. I., *CHEMTECH* **23,** 31 (1993).
8. Schneider, M., and Baiker, A., *in* "Encyclopedia of Advanced Materials" (D. Bloor, R. J. Brook, M. C. Flemings, and S. Mahajan, Eds.) Vol. 1 Pergamon Press, Oxford, 1994.
9. Brinker, C. J., and Scherer, G. W., "Sol–Gel Science, the Physics and Chemistry of Sol–Gel Processing." Academic Press, San Diego, 1990.
10. Scherer, G. W., *J. Am. Ceram. Soc.* **73,** 3 (1990).
11. Armor, J. N., Carlson, E. J., and Carrasquillo, G., *Mater. Lett.* **4,** 373 (1986).
12. Armor, J. N., Carlson, E. J., and Zambri, P. M., *Appl. Catal.* **19,** 339 (1985).
13. Mizushima, Y., and Makoto, H., *Eur. Mater. Res. Soc. Monogr.* **5,** 195 (1993).
14. Asomoza, M., López, T., Gómez, R., and González, R. D., *Catal. Today* **15,** 547 (1992).
15. López, T., Bosch, P., Asomoza, M., and Gómez, R., *J. Catal.* **133,** 247 (1992).
16. López, T., Herrera, L., Gómez, R., Zou, W., Robinson, K., and González, R. D., *J. Catal.* **136,** 621 (1992).
17. Bosch, P., López, T., Lara, V.-H., and Gómez, R., *J. Mol. Catal.* **80,** 299 (1993).
18. López, T., and Gómez, R., *React. Kinet. Catal. Lett.* **49,** 95 (1993).
19. López, T., Villa, M., and Gómez, R., *J. Phys. Chem.* **95,** 1690 (1991).
20. López, T., Mendez-Vivar, J., and Juarez, R., *J. Non-Cryst. Solids* **147 & 148,** 778 (1992).
21. López, T., Gómez, R. Novaro, O., Ramírez-Solís, A., Sánchez-Mora, E., Castillo, S., Poulain, E., and Martínez-Magadán, J. M., *J. Catal.* **141,** 114 (1993).
22. Sen, B., and Vannice, M. A., *J. Catal.* **113,** 52 (1988).
23. Vannice, M. A., and Sen, B., *J. Catal.* **115,** 65 (1989).
24. Raab, C. G., and Lercher, J. A., *Catal. Lett.* **18,** 99 (1993).
25. Coq, B., Tijani, A., Dutartre, R., and Figuéras, F., *J. Mol. Catal.* **79,** 253 (1993).
26. Bankmann, M., Brand, R., Freund, A., and Tacke, T., *Stud. Surf. Sci. Cat.* **78,** 91 (1993).
27. Tauster, S. J., Fung, S. C., Baker, R. T. K., and Horseley, J. A., *Science* **211,** 1121 (1981).
28. Tauster, S. J., *Acc. Chem. Res.* **20,** 389 (1987).
29. Schneider, M., and Baiker, A., *J. Mater. Chem.* **2,** 587 (1992).
30. Thermodynamics Research Center, The Texas A&M University

System, *in* "TRC Thermodynamic Tables—Non-Hydrocarbons," Vol. IV, p. i-5000. College Station, Texas 1992.
31. Thermodynamics Research Center, The Texas A&M University System, *in* "TRC Thermodynamic Tables—Non-Hydrocarbons," Vol. IV, p. i-30. College Station, Texas, 1992.
32. Duff, D. G., Edwards, P. P., Evans, J., Gauntlett, J. T., Jefferson, D. A., Johnson, B. F. G. Kirkland, A. I., and Smith, D. J., *Angew. Chem., Int. Ed. Engl.* **28,** 590 (1989).
33. Hirai, H., Nakao, Y., and Toshima, N., *J. Macromol. Sci., Chem.* **A13,** 727 (1979).
34. Barrett, E. P., Joyner, L. G., and Halenda, P. P., *J. Am. Chem. Soc.* **73,** 373 (1951).
35. Broekoff, J. C. P., *in* "Preparation of Heterogeneous Catalysts" (B. Delmon, P. Grange, P. Jacobs, and G. Poncelet, Eds.), p. 663. Elsevier, Amsterdam, 1979.
36. Harkins, W. D., and Jura, G., *J. Chem. Phys.* **11,** 431 (1943).
37. Klug, H. P., and Alexander, L. E., "X-Ray Diffraction Procedures for Polycrystalline and Amorphous Materials." Wiley, New York, 1974.
38. JCPDS Mineral Powder Diffraction Data File 21-1272, Park Lane, Pennsylvania, 1980.
39. JCPDS Mineral Powder Diffraction Data File 4-0802, Park Lane, Pennsylvania, 1969.
40. Schuck, G. Dietrich, W., and Fricke, J., *in* "Aerogels" (J. Fricke, Ed.), p. 142. Proceedings in Physics, Vol. 6, Springer-Verlag, Berlin, 1986.
41. Sing, K. S. W., Everett, D. H., Haul, R. A. W., Moscou, L., Pierotti, R. A., Rouquérol, J., and Siemieniewska, T., *Pure Appl. Chem.* **57,** 603 (1985).
42. Kirkland, A. I., Edwards, P. P., Jefferson, D. A., and Duff, D. G., *Annu. Rep. Prog. Chem., Sect. C* **87,** 247 (1990).
43. Bhattacharyya, G. K., and Johnson, R. A., "Statistical Concepts and Methods." Wiley, New York, 1977.
44. Prassas, M., Phalippou, J., and Zarzycki, J., *J. Mater. Sci.* **19,** 1656 (1984).
45. Mallát, T., and Petró, J., *Appl. Catal.* **4,** 257 (1982).
46. Scholten, J. J. F., Pijpers, A. P., and Hustings, A. M. L., *Catal. Rev.—Sci. Eng.* **27,** 151 (1985).
47. Thiessen, P. A., *Kolloid-Z.* **101,** 241 (1942).
48. Hunter, R. J., "Foundations of Colloid Science," Vol. 1, p. 97. Oxford Univ. Press, London/New York, 1987.
49. Kim, J.-G., Shyu, J. Z., and Regalbuto, J. R., *J. Catal.* **139,** 153 (1993).
50. Wieckowski, A., *in* "Modern Aspects of Electrochemistry" (R. E. White, J. O'M. Bockris, and B. E. Conway, Eds.), Vol. 21, p. 3. Plenum, New York, 1990.